The Cryosphere Discuss., 8, 3665–3698, 2014
www.the-cryosphere-discuss.net/8/3665/2014/
doi:10.5194/tcd-8-3665-2014

The Cryosphere Discussions
Open Access

Elevation dependency of mountain snow depth

T. Grünewald[1,2], **Y. Bühler**[1], **and M. Lehning**[1,2]

[1]WSL Institute for Snow and Avalanche Research SLF, Flüelastrasse 35, 7260 Davos, Switzerland
[2]Cryos, School of Architecture, Civil and Environmental Engineering, École Polytechnique Fédérale de Lausanne, GRAO 402 – Station 2, 1015 Lausanne, Switzerland

Received: 20 June 2014 – Accepted: 2 July 2014 – Published: 11 July 2014

Correspondence to: T. Grünewald (gruenewald@slf.ch)

Published by Copernicus Publications on behalf of the European Geosciences Union.

Abstract

Elevation strongly affects quantity and distribution of precipitation and snow. Positive elevation gradients were identified by many studies, usually based on data from sparse precipitation stations or snow depth measurements. We present a systematic evaluation of the elevation – snow depth relationship. We analyse areal snow depth data obtained by remote sensing for seven mountain sites. Snow depths were averaged to 100 m elevation bands and then related to their respective elevation level. The assessment was performed at three scales ranging from the complete data sets by km-scale sub-catchments to slope transects. We show that most elevation – snow depth curves at all scales are characterised through a single shape. Mean snow depths increase with elevation up to a certain level where they have a distinct peak followed by a decrease at the highest elevations. We explain this typical shape with a generally positive elevation gradient of snow fall that is modified by the interaction of snow cover and topography. These processes are preferential deposition of precipitation and redistribution of snow by wind, sloughing and avalanching. Furthermore we show that the elevation level of the peak of mean snow depth correlates with the dominant elevation level of rocks.

1 Introduction

Complex orography is the main driving factor for the spatial heterogeneity of precipitation. When advecting moist air masses are blocked by mountains they are forced to ascent at the mountain slopes. Declining air temperatures result in a cooling and a decrease of the saturation pressure of the lifted air parcels. Once the saturation level is reached moisture condensation leads to clouds formation and finally to the onset of precipitation. These processes are enhanced by further lifting which finally results in an increase of precipitation with elevation. However, the interaction of clouds and precipitation particles with the local wind can strongly modify the precipitation patterns at the ground (Mott et al., 2014).

TCD
8, 3665–3698, 2014

Orographic precipitation effects have been studied at a large range of scales for mountain regions all around the world. Most studies identified a distinctive increase of precipitation with altitude (e.g. Spreen, 1947; Peck and Brown, 1962; Frei and Schär, 1998; Blumer, 1994; Johnson and Hanson, 1995; Liu et al., 2011; Asaoka and Kominami, 2012). This positive correlation is also reflected in a general increase of snow depth or snow water equivalent (SWE) as reported by many studies (e.g. Rohrer et al., 1994; Bavera and De Michele, 2009; Lopez-Moreno and Stähli, 2008; Durand et al., 2009; Lehning et al., 2011; Grünewald and Lehning, 2011; Grünewald et al., 2013). Contrary, some studies also report on no or even negative dependencies of elevation and precipitation: for a study site in New Zealand, Kerr et al., 2013 could not identify elevation gradients of SWE and no clear correlations between elevation and SWE were found for some inner-alpine regions in Switzerland (Rohrer et al., 1994). Blumer (1994), Basist et al. (1994) and Arakawa and Kitoh (2011) even reported on negative elevation gradients of precipitation.

Consequently the shape of the elevation – precipitation relation can vary strongly even over small distances (e.g. Lauscher, 1976; Rohrer et al., 1994; Basist et al., 1994; Sevruk, 1997; Wastl and Zängl, 2008). This strong variability is attributed to the highly complex interaction of the weather patterns with the local topography. Sevruk (1997) speculates that “in a series of inner-alpine valleys following each other and having different orientation, slopes and altitude, the redistribution of precipitation by wind can be the dominant factor of its spatial distribution suppressing any other effects including the altitude". Other studies postulate an advective leeward shift of the local precipitation maximum, favoured by specific topographical and meteorological conditions (Carruthers and Choularton, 1983; Robichaud and Austin, 1988; Zängl, 2008; Zängl et al., 2008; Mott et al., 2014). Due to its lower fall speed, this shift is more pronounced for snow fall than for rain (Colle, 2004; Zängl, 2008). On a smaller scale, Mott et al. (2014) showed that orographically modified patterns of mean horizontal and vertical wind velocities affect particle trajectories inducing reduced snow deposition rates on windward slopes and enhanced deposition on leeward slopes. Small-scale snowfall patterns over

TCD
8, 3665–3698, 2014

single inner-alpine mountain peaks can, thus, differ significantly from those observed on a larger scale for large mountain ranges, where cloud formation processes tend to make the leeward slopes drier than windward slopes (Houze, 2012; Mott et al., 2014). The thickness of the snow cover at the end of the winter season can serve as a proxy for the seasonally accumulated precipitation on the ground. However, Scipion et al. (2013) identified large differences between precipitation patterns obtained by a high resolution Doppler X-band radar and the final seasonal snow accumulation. These differences are attributed to several processes that affect the snow once on the ground: due to gravitational forces snowflakes might immediately glide downslope if they land on sufficiently sloped surfaces. Furthermore the wind can redistribute the snow from exposed to sheltered locations (Gauer, 2001; Mott et al., 2010). The erosion by the wind is largest at higher altitudes as wind speeds and exposure tend to increase with elevation. Moreover, driven by gravitation, snow is potentially moved downward by creeping, sloughing and avalanching (Bernhardt and Schulz, 2010; Gruber, 2007). Finally snow melt, sublimation and phase transitions from snow to rain, especially in spring might affect the snow amount, particular in lower elevations (Elder et al., 1991). In combination, these processes modify the elevation driven precipitation signal stored in the snow cover. As a rough summary, reduced snow amounts at the crest level, in steep slopes and the lowest elevations are contrasted by enhanced accumulation in flat and protected areas at the slope toes.

As most of the studies mentioned before are based on a limited number of gauges or weather stations, the potential bias of the results appears relatively large (Havlik, 1969; Sevruk, 1997). Inadequate spatial station coverage, especially in high altitudes (Blanchet et al., 2009; Daly et al., 2008; Sevruk, 1997; Wastl and Zängl, 2008) and the large potential measurement error of precipitation, especially in exposed areas (Rasmussen et al., 2001, 2011; Sevruk, 1997; Yang et al., 1998) are important factors that might have an impact on the results of these studies. In contrast, owing to the rapid development of remote sensing techniques such as laser scanning (LiDAR), high spatial resolution data sets have recently become available for the snow cover (e.g.

TCD
8, 3665–3698, 2014

Deems et al., 2013; Grünewald et al., 2010, 2013). Furthermore, significant advances in the development and application of Doppler radars for precipitation quantification have been reported (Scipion et al., 2013; Mott et al., 2014). However, the resolution of these systems is still insufficient to reflect the small scale variability of precipitation and snow fall close to the surface.

To our knowledge the only systematic study on elevation gradients of snow that is based on such area-wide data has been presented by Grünewald and Lehning (2011). They compared elevation gradients calculated from airborne LiDAR surveys with simple climatological and snow station based gradients for two small study sites in the Eastern Swiss Alps. Principally Grünewald and Lehning (2011) identified a positive correlation of SWE and elevation but they also recognised strong deviations between the two sites, two consecutive years and between the three different approaches. For the LiDAR gradients they found that the relation between elevation and snow depth levelled at a certain altitude and finally even decreased. From this finding the question arose, if such a shape is generally characteristic for the snow depth elevation relationship.

The availability of a large data set consisting of area-wide high resolution snow depth data from different mountain regions (Grünewald et al., 2013) now allows us to test this hypothesis. Based on Grünewald and Lehning (2011) we systematically analyse snow depth elevation gradients for different scales ranging from slope transects to the entire catchments or mountain sites. In addition to the identification of typical shapes we also aim to explain the location of the previously mentioned maximum of the relation between elevation and snow depth.

TCD
8, 3665–3698, 2014

2 Data

2.1 Airborne laser scanning (ALS)

Recent years have seen an increasing number of applications of airborne laser altimetry (ALS or LiDAR) for snow studies (e.g. Deems et al., 2006, 2008; Grünewald et al., 2013; Grünewald and Lehning, 2011; Lehning et al., 2011; Trujillo et al., 2007, 2009). High resolution snow depth maps are calculated by subtracting two digital surface models (DSM), one obtained in snow-covered and one in snow-free conditions. It has been shown that ALS is a valid method for gathering area-wide snow depth data (e.g. Hopkinson et al., 2004; Deems and Painter, 2006; Deems et al., 2013) and that vertical accuracies are in the range centimetres to few decimetres (Grünewald et al., 2010; Bollmann et al., 2011; Hopkinson et al., 2012; Deems et al., 2013). In principal, data sets obtained by helicopter-based LiDAR appear to be more accurate than data sets gathered from aeroplanes (Grünewald et al., 2013). This is attributed to reduced flying height, terrain-following flight line of the helicopter and a better footprint in steep terrain due to the tilting sensor. A detailed review on ALS for snow cover observations has recently been published by Deems et al. (2013). Additionally, more general information can be found in Baltsavias (1999) and Wehr and Lohr (1999). The ALS data sets analysed in this study and how they were processed is comprehensively described in Grünewald et al. (2013).

2.2 Airborne digital photogrammetry (ADP)

Airborne digital photogrammetry (ADP) is a remote sensing technology that is applied to acquire high resolution DSMs by exploiting photogrammetric image correlation techniques (Maune, 2001). Identical to ALS, snow depth maps can be calculated by subtracting a summer DSM from a winter DSM.

The Leica Geosystems Airborne Digital Sensor ADS80 (Fig. 1) is an opto-electronic line scanner mounted on an aeroplane, that is able to simultaneously acquire four

TCD
8, 3665–3698, 2014

spectral bands (red, green, blue and near infrared) with a radiometric resolution of 12 bits from three different viewing angles. GNSS/IMU supported orientation of the image strips supplemented by the use of ground control points achieved a horizontal accuracy of 1–2 ground sampling distances (0.25–0.5 m). The sensor had already been successfully used to detect avalanche deposits in the area of Davos (Bühler et al., 2009) and is more economic for large-scale data aquisition than ALS due to higher flight altitude and therefore reduced flight time. More detailed information on the Leica ADS opto-electronic scanner can be found in Sandau (2010).

In this study we apply snow depth maps in 2 m resolution produced by Bühler et al. (2014). Areas covered by forests, bushes and buildings as well as identified outliers are masked out prior to the snow depth map generation because the reliability of the DSM is substantially reduced in those areas. Bühler et al. (2014) compared the ADS snow depth maps with different independent snow depth measurements. They find RMSE values of less than 30 cm in areas above tree line. The RMSE values strongly depend on the distance of the sensor to the ground which reduces the accuracy of snow depth to less than 50 cm at the valley bottom (highest distances). Moreover Bühler et al. (2012) found that the quality of the data is limited by the steepness of the terrain. They state that data gathered in slopes steeper than 50° might be affected by large potential biases.

3 Study sites

Basic descriptions and some summary statistics on topography and snow cover of the investigation areas are provided in Tables 1 and 2. Apart from the ADS-data, the data sets analysed in this study are the same as in Grünewald et al. (2013). We are therefore only proving a very short overview on each of the study sites.

A large data set has been collected by ADS for the district of Davos in the eastern part of the Swiss Alps at 3 September 2013 and 20 March 2012 (Fig. 2). In total an area of 124 km^2 consisting of 12 overlapping image strips (approx. 70 % overlap across

TCD
8, 3665–3698, 2014

track) has been covered in the surveys. The ground sampling distance of the imagery is about 25 cm, limited through the minimal flying height for high alpine terrain (Bühler et al., 2012).

The data set has been split into two study sites: the Strela data set (STRE) covers a large section of the mountain range located in the Northwest of the Landwasser valley (Figs. 2 and 3c). The mountain range spans from Southwest to Northeast and is perpendicular to the main wind that is typically from the Northwest (Schirmer et al., 2011). Northern and southern aspects are dominant in the data. The terrain is a mixture of alpine slopes with varying steepness. Rocky outcrops and some larger rock faces are present, especially in the summit regions. Note that the Wannengrat data set (WAN) is a small subsection in the centre of STRE. However the year of the survey and the sensor obtained for the data collection differ (Table 1).

The second study site in the region of Davos is the Dischma valley (DIS) in the East of the town of Davos (Figs. 2 and 3a). The 13 km long valley extends parallel to the main flow from the Northwest to the Southeast. The data set is not only consisting of the eastern and western slopes of the Dischma valley but also includes the upper flanks of the two neighbouring valleys. The land cover is similar to STRE but easterly and westerly aspects are dominating. Two summer season were between the summer (September 2013) and the winter survey (March 2012) applied for the snow depth calculation. As we cannot account for potential changes of the glacier surface in summer, that could bias the snow depth on the glaciers, we removed the two small glaciers in the highest elevation of the site.

This large data set is supplemented by the smaller, ALS based data sets presented by Grünewald et al. (2013) (Tables 1 and 2). The Piz Lagrev (LAG) is a steep, south-facing mountain slope in the Engadine valley in the Southeast of Switzerland. The area is dominated by steep rock-faces and two rather flat bowls where most of the snow accumulates. The Haut Glacier d'Arolla (ARO) is located in the western part of the Swiss Alps. About half of the site is covered by glaciers. The remaining areas are rather steep talus slope and rock-faces. The characteristics of the Hintereisferner

TCD
8, 3665–3698, 2014

(HEF) study domain in the Öztal Alps of southwestern Austria are similar to ARO. Steep talus slopes and rock-faces dominate the valley flanks and about 50 % of the domain is glaciated. The last study site analysed in this paper is the Vall de Núria located at the main divide of the eastern Spanish Pyrenees. Slopes of diverse steepness with some rocky outcrops near the summit level are typical of this 28 km^2 data set.

4 Methods

This study analyses elevation dependencies of snow depth at three different scales. First regional characteristics are assessed by calculating gradients for the complete data sets listed in Table 2. Secondly, we subdivided the data into smaller sub-catchments (1 to 5 km^2) as shown in Figs. 2 and 3a, c. This gives a measure of the variability. To assess the scale of single mountain slopes, we manually defined 100 m wide transects (Fig. 3). These transects extend perpendicular to the slope and span the entire difference in altitude of the respective mountain slopes.

Similar as in Grünewald and Lehning (2011) the subareas were subdivided into 100 m elevation bands and the mean snow depth was calculated for each subarea and each elevation zone. To avoid values that are based on a very small number of cells, elevation zones that had less than 0.5 % of the total number of cells of the specific sub-catchment or transect were removed. The mean snow depths were then plotted against their respective elevation level and classified according to their general shape. Based on a first visual analysis we identified a set of typical shapes of gradients as indicated in Fig. 4 and discussed below. For all curves that were characterised by a distinctive peak (Fig. 4 shape A and B), that reflects a local maximum of the elevation – snow depth relationship, the elevation level of this peak was detected.

A visual examination of the location of the peak in relation to the topography of the subarea suggests a possible correlation with the elevation level of distinctive rocky outcrops (level of rocks). The lower elevation levels of such rocky sections were therefore, where present, manually identified from topographic maps or hillshade-images and

TCD
8, 3665–3698, 2014

rounded to the nearest 50 m contour line. This procedure works well for transects but is rather vague at the scales, where large areas are included in each elevation zone. This leads to large potential scatter of the level of rocks. While relatively clear levels could be detected for most slope transects, the rocky sections already varied strongly for the sub-catchments. At the scale of entire valleys or mountain ranges (data sets), the even larger diversity fully prevents an identification of a single rock level. Finally, it needs to be noted that such rocky sections were not present for all subareas. For the subareas that featured both, a peak and a clear level of rock, we finally created scatter plots and correlation analysis. This was on the one hand performed for each of the study areas separately and on the other hand for the comprehensive data set.

5 Results

5.1 General shape of gradients

Figure 4 indicates idealised shapes of the elevation – snow depth relationships as qualitatively detected from the data (Figs. 5, 6 and 7). The most prominent shape is shown in panel A of Fig. 4: the curve increases up to a specific elevation level where it peaks and finally decreases in the remaining elevation bands. Note that this shape is an oversimplification that only aims to picture the main characteristics of the general shapes. The slope is not necessarily steady, several smaller spikes and peaks might be present and the peak of the gradient can be flat and span several elevation bands. Figures 5 to 7 are examples for the variability of the single shapes.

Panels B to E of Fig. 4 illustrate variations of type A. Type B is principally identical to A but is additionally characterised by a dominant snow depth maximum in the lowest elevations. Such maxima are caused by local accumulation zones such as snow filled ditches or avalanche depositions. A distinctive secondary maximum is always present in class B. For the analysis presented in 5.6, this secondary maximum is treated as peak of the elevation – snow depth relationship. Gradients classified as type C to E

TCD
8, 3665–3698, 2014

do not show distinctive peaks. C is similar to B but a decrease of snow depth in the higher elevations is missing. Shape D and E present steady positive (D) or negative (E) gradients with no clear maximum. These variations are attributed to processes in the discussion below.

Figure 5a presents elevation gradients of snow depth for the entire data sets. For Fig. 5b, the curves were normalised according to:

$$\tilde{X} = \frac{X - \min(X)}{\max(X) - \min(X)} \quad (1)$$

where $\tilde{X}$ represents the scaled variable (snow depth or elevation).

5.2 Gradients: entire data sets

At the scale of the entire data sets, we only detected type A gradients (Fig. 5). This shape is evident for the raw data (Fig. 5a) and the curves show a fairly nice collapse in the rescaled data (Fig. 5b). All data sets show a clear increase of snow depth with elevation followed by a pronounced maximum and a more or less definitive decrease. Even though the general shape appears similar, the location of the maximum and the gradient appear variable between the study sites.

5.3 Gradients: sub-catchment

Figure 6 presents curves for five selected sub-catchments for STRE (Fig. 6a) and DIS (Fig. 6b) respectively. The locations of the sub-catchments are indicated in Fig. 3. Most of the curves can be classified as type A (CS1, CS3, and CD2 to 5) but the shapes are more variable than on the scale of the entire data sets (Fig. 5). Mean snow depths are clearly increasing with elevation and reach pronounced peaks at a certain level.

CS2, CS4, CS5 and CD1 are representative for type B gradients: a maximum in the lowest elevation band is followed by a short negative trend and a steady increase culminating in a distinct peak. The maxima at the low elevation bands are attributed to

TCD
8, 3665–3698, 2014

snow filled ditches that dominate the largest portion of the lowest elevation bands. The combination of a relatively small area of the elevation zone (in comparison to the other zones of the sub-catchments) with snow depths of more than five metres in the gullies explains the low maxima for CS4 and CS5. The accumulation zone in and around a ditch in CS2, with snow depths around 2 m, is clearly less pronounced than those in CS4 and CS5. However, this small area of snow accumulation is still enough for the slight maximum in comparison to the shallower snow depth in the higher elevation zones. The extreme snow depths in CD1 are caused by the deposition of large snow drift in a terrain depression at the foot of the steep northern slopes. This accumulation zone is covering the vast part of the two lower elevation bands and snow depths of more than eight metres could be detected. Depositions of similar dimensions are also present in some of the higher elevation bands. However, they do not cover such large portions of the area as in the lower section. This results in the clearly reduced mean values and in the decreasing trend of the black curve (CD1) in Fig. 6b. Above the low-elevation maxima typical type A shapes are evident for CS2, CS4, CS5 and CD1.

5.4 Gradients: slope-transects

Figure 7 displays identical relations as Fig. 6 but for transects instead of sub-catchments. The shapes of the curves show a higher variability in Fig. 7 than those in Figs. 5 and 6. This is because the slighter support areas of each elevation band provoke larger effects of the small scale variability in snow depth on the shape of the curves. In contrast this small scale heterogeneity is rather smoothed out for the sub-catchment (Fig. 6) or the complete data sets (Fig. 5). However, the principal findings are also visible for the transects. Most of the curves can be classified as type A (TS2, TS3, TS4, TS5, TD1, TD2, TD3, TD5). TS2 displays nearly an ideal type A (Fig. 4) curve with a linear increase, followed by a marked snow depth maximum at 2450 m. Contrary, the maximum of TS3 appears less pronounced. The detailed map of the two transects (Fig. 3d) provides insight into the snow cover characteristics that cause the respective curves. Little snow in the lower sections, the location of the maxima in the

TCD
8, 3665–3698, 2014

flat bowls and the decrease of snow depth in the steep, rocky slopes at the highest elevations are clearly visible. A second detailed map is illustrated in Fig. 3b for TD1 and TD2. Again, the pronounced peaks and the distinct decrease of snow in the steep rock bands at the top levels are well illustrated. The curve with the most extreme maximum is represented by TS4 (Fig. 7a). While only little snow had been accumulated on the rock-face itself, a large deposition zone is evident in the gentle slope at the foot of the rock-face (Fig. 3c). Redistribution of snow due to gravitational forces might be the main cause for these extreme snow depth differences.

Different types of shape are only present for TS1 and TD4. TS1 represents a type C curve with a low peak, a distinctive minimum and a slightly denoted secondary peak in the higher elevation. The low maximum is attributed to a snow filled ditch in the lowest elevations and the secondary peak is caused by an accumulation zone in a gentle bowl below steep slopes at the top. TD4 has been classified as type D. The curve is characterised by predominately positive slopes with two smaller peaks and a maximum in the highest elevation zone.

5.5 Frequency distribution of gradient types

Figure 8 summarises the number of subareas that have been assigned to the specific type of gradient for each data set. 67 to 100 % of all gradients have been classified as type A for the sub-catchments of each specific study site (Fig. 8a). In total 79 % of all sub-catchments belong to type A. Merging all gradients with a distinctive peak (type A and B) increases the portion to 93 %. All other types appear to be rare. Only one sub-catchment in DIS has been classified as type C and one in each case for NUR and STRE. A similar picture characterises the distribution of the gradient types at the scale of the transects (Fig. 8b). 72 % of all transects (60 to 89 % of each data set) belong to type A. Combining type A and B results in an increase to 79 %. Similar to Fig. 8a, the remaining types are very rare. Only type D (positive trend) curves are more frequent, at least for DIS and STRE.

TCD
8, 3665–3698, 2014

5.6 Relation of elevation gradients and topography

In the previous section we have shown that the vast majority of subareas feature distinctive maxima in their elevation – snow depth relationships. From this finding, the question whether the elevation level of this peak can be explained by the topographical settings of its respective location should be answered. Visual impression suggests that most of the maxima would be found below distinctive terrain breaks such as steep cliffs or slopes. We tried to automatically identify the elevation of the most dominant terrain break for each subarea by calculating the maximum inclination of the relationship between elevation and terrain slope and terrain roughness (expressed by the standard deviation of the slope) respectively. However, the topographical complexity of the terrain prevented an adequate identification of the appropriate elevation level. This is also reflected in the correlation of these measures with the elevation levels of the maxima of the elevation – snow depth relationships that were relatively low. Following this, we manually identified the predominant level of rocks as described before.

A rock level was present for the majority of the subareas (transects: 70 %, sub-catchments: 71 %). In total 67 % of the sub-catchments and 58 % of the transects feature both, a peak in the elevation – snow depth curves (Fig. 8 shape A and B) as well as a level of rocks.

Figure 9 illustrates scatter-plots of the level of rocks versus the level of the maximum of the elevation – snow depth relationship. Especially for the transects (Fig. 9b) a clear linear relationship ($R^2 = 0.84$) is visible. Such a correlation is present for each single data set and for the merged data. Figure 9b also indicates that the vast majority of the points are shifted by about 50 to 200 m below the 1-1 line. Hence, the areas with the peak in the snow depths tend to be located below the level of rocks. This confirms the expectation that more snow tends to accumulate in gentle slopes at the foot of steep slopes and rough terrain due to preferential deposition (Lehning et al., 2008) and redistribution of snow by sloughing, avalanching and wind drift. The two outliners for HEF (dark blue circles at the right side of Fig. 9b) are transects that span the entire

TCD
8, 3665–3698, 2014

glacier. Rocks are only present in the highest elevation bands. The snow depth maxima are located at accumulation zones in the middle elevations of the glacier. A secondary, less pronounced peak was found below this rock band but is not visible in Fig. 9b. The two positive outlier of NUR (light blue circles at the left side of Fig. 9b) can also be explained by their specific topography: a small rock band is present in both transects but the main peak in the elevation – snow depth curve can be found in a flatter section on top of the rock face. Removing these four outliers would increase R^2 to 0.9.

In contrast to Fig. 9b the correlation ($R^2 = 0.37$) for the sub-catchments (Fig. 9a) – even though still highly significant – appears much weaker. A downward shift as notified for the transects is not evident. As described before, the reason for this reduced correlation is probably that the level of rock cannot be clearly detected for such large areas. Moreover, the mean snow depths in each elevation band rather reflect the average of large areas with variable topography and not of a clearly differentiated terrain unit as for the transects. In combination, this higher variability counteracts the predictability of the location of the peak.

6 Discussion

We have shown that the vast majority of subareas are characterised by positive elevation gradients of snow depth with distinct peaks at a certain level. This finding is valid for all investigation areas and at all scales even though the effect was less universal for smaller subareas (transects). We suggest that this shape is attributed to a principal positive elevation gradient of precipitation that is modified by the interaction of the snow cover with the local terrain. Processes that reshape the precipitation distribution near the surface and the snow accumulation at the ground are first the preferential deposition of precipitation in sheltered areas and secondly the redistribution of snow by wind and gravity. These processes result in a relocation of snow from steep and exposed areas to rather sheltered gentle slopes in lower elevations. Such steep, exposed and frequently rocky areas are usually located in the highest elevations (at least for the data

TCD
8, 3665–3698, 2014

sets analysed in this study). This interpretation is well confirmed by our results. Hence, our results are in agreement with findings of earlier studies. Most of them reported on positive gradients of precipitation (e.g. Spreen, 1947; Peck and Brown, 1962; Frei and Schär, 1998; Blumer, 1994; Johnson and Hanson, 1995; Liu et al., 2011; Asaoka and Kominami, 2012) and snow (e.g. Rohrer et al., 1994; Bavera and De Michele, 2009; Lopez-Moreno and Stähli, 2008; Grünewald and Lehning, 2011; Lehning et al., 2011; Grünewald et al., 2013). Nevertheless, we also show that the elevation – snow depth relation can vary significantly even at small distances and that areas of negative gradients are also existing. Such variability had also been postulated in earlier publications (e.g. Lauscher, 1976; Rohrer et al., 1994; Basist et al., 1994; Sevruk, 1997; Wastl and Zängl, 2008).

We acknowledge the previously mentioned limitation in reliability of the data in extremely steep slopes. This constraint is especially affecting the ADP data (Bühler et al., 2012) but must also be considered for the ALS data, especially for HEF and NUR, that had been obtained on aeroplane-based platforms (Bollmann et al., 2011; Hopkinson et al., 2012). However, the relatively small portion of such steep slopes in the data strongly limits the influence of such cells on the presented analysis. Only about 5 % of the cells in DIS, STRE and HEF (2 % of NUR) are steeper than 50° and less than 2 % are steeper than 60°. For STRE and HEF about one third of these steep (> 50°) cells had already been masked in the post-processing of the data. Following this, the reduced accuracy of extremely steep areas will only have a minor impact on analysis of larger subareas (entire data sets and sub-catchments). Contrary, for transects, large portions of elevation bands that coincide with pronounced rock-faces are present. However, a detailed examination of such sections did not yield any conspicuous outcome. As the results agree with our principal process understanding we are confident that the findings are adequate, especially as the focus of the analysis is rather qualitative.

TCD
8, 3665–3698, 2014

7 Conclusions

We present a detailed assessment of the relationship of snow depth and elevation. The analysis is based on an extensive, spatial continuous data set consisting of high resolution and high quality snow depth data from seven mountain sites in the European Alps and Spanish Pyrenees. All data sets were gathered near to the maximum of the winter accumulation of the respective site and year. The analysis is performed on three different scales that range from basements or mountain ranges (entire data sets) to sub-catchments (km-scale) and individual slope transects.

We show that a characteristic shape of the elevation – snow depth relation was evident for the majority of the subareas at all scales. Typically, snow depth increases with elevation up to a certain level where a distinct peak can be found. Following this maximum, the mean snow depth tends to significantly decrease for the highest elevations (type A in Fig. 4). At the mountain range scale all data sets showed the characteristic type A curve. 79 % of the sub-catchments and 72 % of the transects belong to this type. Merging the two types that are characterised by a distinct peak (A and B) increases the portion to 93 % for the sub-catchments and 79 % for the transects. However, the detailed shapes of the gradients are still variable. Location and shape of the peak and the slope of the curves differ between the subareas. Curves that deviate from this general shape are sparse but present.

We attribute this typical shape to an increase of snow fall with elevation. Snow depths are reshaped by redistribution of snow by wind and gravitational forces. In combination, these processes determine the typical shape of the gradients. In how far already the expected decrease in total precipitation/snow fall with altitude (e.g. Blanchet et al., 2009) is playing a role remains to be investigated in future.

This interpretation is fortified by an examination of the topographical location of these peaks. This analysis showed that a high correlation between the elevation of the peak and – if present – the level of predominant rocks exists. For the transects the maximum of the elevation – snow depth relationship tends to be located 50 to 200 m below the

TCD
8, 3665–3698, 2014

level of rocks. Note that this study is restricted to a fistful of selected study sites and single dates in a solitary year. The transferability of the results to other years remains limited, even though several studies have identified a high temporal consistency of snow depth between different seasons (Deems et al., 2008; Schirmer et al., 2011; Helfricht et al., 2014). However, it may not be assumed that such a consistency is valid for all mountain sites. Moreover, we analysed snow depth data that reflect a cumulative snow accumulation record of an entire accumulation season. Elevation gradients of single precipitation events might deviate from the patterns averaged for a complete accumulation season.

Acknowledgements. The Swiss National Foundation is acknowledged for partly funding this work. We furthermore thank all our colleagues who helped in various ways, especially R. Mott, M. Marty and C. Ginzler. Finally, we are grateful to all people and institutions who provided data, particularly, Leica Geosystems for the ADP data, the Amt für Wald und Naturgefahren Graubünden for financial support for the LAG and WAN data, I. Moreno Banos, P. Oller, J. Marturia (Institut Geologic de Catalunia) for the NUR data, H. Stötter (Institute for Geography, University of Innsbruck) for the HEF data and R. Dadic (Antarctic Research Centre, University of Wellington) and P. Burlando (Institute for Environmental Engineering, ETH Zurich) for the data sets from ARO.

References

Arakawa, O. and Kitoh, A.: Intercomparison of the relationship between precipitation and elevation among gridded precipitation datasets over the Asian summer monsoon region, Global Environ. Res., 15, 109–118, 2011. 3667

Asaoka, Y. and Kominami, Y.: Spatial snowfall distribution in mountainous areas estimated with a snow model and satellite remote sensing, Hydrol. Res. Lett., 6, 1–6, 2012. 3667, 3680

Baltsavias, E.: Airborne laser scanning: basic relations and formulas, J. Photogr. Remote Sens., 54, 199–214, 1999. 3670

Basist, A., Bell, G. D., and Meentemeyer, V.: Statistical relationships between topography and precipitation patterns, J. Climate, 7, 1305–1315, doi:10.1175/1520-0442(1994)007<1305:srbtap>2.0.co;2, 1994. 3667, 3680

Bavera, D. and De Michele, C.: Snow water equivalent estimation in the Mallero basin using snow gauge data and MODIS images and fieldwork validation, Hydrol. Process., 23, 1961–1972, doi:10.1002/hyp.7328, 2009. 3667, 3680

Bernhardt, M. and Schulz, K.: SnowSlide: a simple routine for calculating gravitational snow transport, Geophys. Res. Lett., 37, L11502, doi:10.1029/2010gl043086, 2010. 3668

Blanchet, J., Marty, C., and Lehning, M.: Extreme value statistics of snowfall in the Swiss Alpine region, Water Resour. Res., 45, 12, W05424, doi:10.1029/2009wr007916, 2009. 3668, 3681

Blumer, F.: Höhenabhängigkeit des Niederschlags im Alpenraum, Ph. D. thesis, Zurich, ETH Zurich, 1994. 3667, 3680

Bollmann, E., Sailer, R., Briese, C., Stotter, J., and Fritzmann, P.: Potential of airborne laser scanning for geomorphologic feature and process detection and quantifications in high alpine mountains, Z. Geomorphol., 55, 83–104, doi:10.1127/0372-8854/2011/0055s2-0047, 2011. 3670, 3680, 3688

Bühler, Y., Hüni, A., Christen, M., Meister, R., and Kellenberger, T.: Automated detection and mapping of avalanche deposits using airborne optical remote sensing data, Cold Reg. Sci. Technol., 57, 99–106, doi:10.1016/j.coldregions.2009.02.007, 2009. 3671, 3688, 3690

Bühler, Y., Marty, M., and Ginzler, C.: High resolution DEM generation in high-alpine terrain using airborne remote sensing techniques, Trans. GIS, 16, 635–647, doi:10.1111/j.1467-9671.2012.01331.x, 2012. 3671, 3672, 3680

Bühler, Y., Marty, M., Egli, L., Veitinger, J., Jonas, T., Thee, P., and Ginzler, C.: Spatially continuous mapping of snow depth in high alpine catchments using digital photogrammetry, The Cryosphere Discuss., 8, 3297–3333, doi:10.5194/tcd-8-3297-2014, 2014. 3671, 3688

Carruthers, D. J. and Choularton, T. W.: A model of the feeder-seeder mechanism of orographic rain including stratification and wind-drift effects, Q. J. Roy. Meteor. Soc., 109, 575–588, doi:10.1002/qj.49710946109, 1983. 3667

Colle, B. A.: Sensitivity of orographic precipitation to changing ambient conditions and terrain geometries: an idealized modeling perspective, J. Atmos. Sci., 61, 588–606, doi:10.1175/1520-0469(2004)061<0588:SOOPTC>2.0.CO;2, 2004. 3667

Dadic, R., Mott, R., Lehning, M., and Burlando, P.: Wind influence on snow depth distribution and accumulation over glaciers, J. Geophys. Res.-Earth, 115, F01012, doi:10.1029/2009JF001261, 2010a. 3688

TCD
8, 3665–3698, 2014

Dadic, R., Mott, R., Lehning, M., and Burlando, P.: Parameterization for wind-induced preferential deposition of snow, Hydrol. Process., 24, 1994–2006, doi:10.1002/hyp.7776, 2010b. 3688

Daly, C., Halbleib, M., Smith, J. I., Gibson, W. P., Doggett, M. K., Taylor, G. H., Curtis, J., and Pasteris, P. P.: Physiographically sensitive mapping of climatological temperature and precipitation across the conterminous United States, Int. J. Climatol., 28, 2031–2064, doi:10.1002/Joc.1688, 2008. 3668

Deems, J. S. and Painter, T. H.: Lidar measurement of snow depth: accuracy and error sources, in: Proceedings International Snow Science Workshop ISSW 2006, Telluride, CO, Proceedings International Snow Science Workshop ISSW, 384–391, 1–6 October 2006, Telluride, CO, USA, 2006. 3670

Deems, J. S., Fassnacht, S. R., and Elder, K. J.: Fractal distribution of snow depth from Lidar data, J. Hydrometeorol., 7, 285–297, 2006. 3670

Deems, J. S., Fassnacht, S. R., and Elder, K. J.: Interannual consistency in fractal snow depth patterns at two Colorado mountain sites, J. Hydrometeorol., 9, 977–988, doi:10.1175/2008jhm901.1, 2008. 3670, 3682

Deems, J. S., Painter, T. H., and Finnegan, D. C.: Lidar measurement of snow depth: a review, J. Glaciol., 59, 467–479, doi:10.3189/2013JoG12J154, 2013. 3669, 3670

Durand, Y., Giraud, G., Laternser, M., Etchevers, P., Mèrindol, L., and Lesaffre, B.: Reanalysis of 47 years of climate in the French Alps (1958–2005): climatology and trends for snow cover, J. Appl. Meteorol. Clim., 48, 2487–2512, doi:10.1175/2009jamc1810.1, 2009. 3667

Elder, K., Dozier, J., and Michaelsen, J.: Snow accumulation and distribution in an Alpine watershed, Water Resour. Res, 27, 1541–1552, doi:10.1029/91wr00506, 1991. 3668

Frei, C. and Schär, C.: A precipitation climatology of the Alps from high-resolution rain-gauge observations, Int. J. Climatol., 18, 873–900, 1998. 3667, 3680

Gauer, P.: Numerical modeling of blowing and drifting snow in Alpine terrain, J. Glaciol., 47, 97–110, 2001. 3668

Geist, T. and Stötter, J.: Documentation of glacier surface elevation change with multi-temporal airborne laser scanner data – case study: Hintereisferner and Kesselwandferner, Tyrol, Austria, Zeitschr. Gletscherk. Glazialgeol., 41, 77–106, 2008. 3688

Gruber, S.: A mass-conserving fast algorithm to parameterize gravitational transport and deposition using digital elevation models, Water Resour. Res., 43, W06412, doi:10.1029/2006wr004868, 2007. 3668

TCD
8, 3665–3698, 2014

Grünewald, T. and Lehning, M.: Altitudinal dependency of snow amounts in two small alpine catchments: can catchment-wide snow amounts be estimated via single snow or precipitation stations?, Ann. Glaciol., 52, 153–158, 2011. 3667, 3669, 3670, 3673, 3680, 3688

Grünewald, T., Schirmer, M., Mott, R., and Lehning, M.: Spatial and temporal variability of snow depth and ablation rates in a small mountain catchment, The Cryosphere, 4, 215–225, doi:10.5194/tc-4-215-2010, 2010. 3669, 3670

Grünewald, T., Stötter, J., Pomeroy, J. W., Dadic, R., Moreno Baños, I., Marturià, J., Spross, M., Hopkinson, C., Burlando, P., and Lehning, M.: Statistical modelling of the snow depth distribution in open alpine terrain, Hydrol. Earth Syst. Sci., 17, 3005–3021, doi:10.5194/hess-17-3005-2013, 2013. 3667, 3669, 3670, 3671, 3672, 3680

Havlik, D.: Die Höhenstufe maximaler Niederschlagssummen in den Westalpen: Nachweis und dynamische Begründung, 1–76 pp., 1969. 3668

Helfricht, K., Schöber, J., Schneider, K., Sailer, R., and Kuhn, M.: Inter-annual persistence of the seasonal snow cover in a glacierized catchment, J. Glaciol., submitted, 2014. 3682

Hopkinson, C., Sitar, M., Chasmer, L., and Treitz, P.: Mapping snowpack depth beneath forest canopies using airborne lidar, Photogramm. Eng. Rem. S., 70, 323–330, 2004. 3670

Hopkinson, C., Collins, T., Anderson, A., Pomeroy, J., and Spooner, I.: Spatial snow depth assessment using LiDAR transect samples and public GIS data layers in the Elbow River Watershed, Alberta, Can. Water Resour. J., 37, 69–87, doi:10.4296/cwrj3702893, 2012. 3670, 3680

Houze, R. A.: Orographic effects on precipitating clouds, Rev. Geophys., 50, RG1001, doi:10.1029/2011rg000365, 2012. 3668

Johnson, G. L. and Hanson, C. L.: Topographic and atmospheric influences on precipitation variability over a mountainous watershed, J. Appl. Meteorol., 34, 68–87, doi:10.1175/1520-0450-34.1.68, 1995. 3667, 3680

Lauscher, F.: Weltweite Typen der Höhenabhängigkeit des Niederschlags, Wetter und Leben, 28, 80–90, 1976. 3667, 3680

Lehning, M., Löwe, H., Ryser, M., and Raderschall, N.: Inhomogeneous precipitation distribution and snow transport in steep terrain, Water Resour. Res., 44, W07404, doi:10.1029/2007wr006545, 2008. 3678

Lehning, M., Gruenewald, T., and Schirmer, M.: Mountain snow distribution governed by an altitudinal gradient and terrain roughness, Geophys. Res. Lett., 38, L19504, doi:10.1029/2011GL048927, 2011. 3667, 3670, 3680, 3688

TCD
8, 3665–3698, 2014

Liu, C., Ikeda, K., Thompson, G., Rasmussen, R., and Dudhia, J.: High-resolution simulations of wintertime precipitation in the Colorado headwaters region: sensitivity to physics parameterizations, Mon. Weather Rev., 139, 3533–3553, doi:10.1175/mwr-d-11-00009.1, 2011. 3667, 3680

Lopez-Moreno, J. I. and Stähli, M.: Statistical analysis of the snow cover variability in a subalpine watershed: Assessing the role of topography and forest, interactions, J. Hydrol., 348, 379–394, doi:10.1016/j.jhydrol.2007.10.018, 2008. 3667, 3680

Maune, D.: Digital Elevation Model Technologies and Applications: The DEM Users Manual, American Society for Photogrammetry and Remote Sensing, Bethesda, MD, 2001. 3670

Moreno Baños, I., , Ruiz Garcia, A., Marturià, Alavedra, J., Oller I Figueras, P., Pina Iglesias, J., Garcia Selles, C., Martinez I Figueras, P., and Talaya Lopez, J.: Snowpack depth modelling and water availability from LIDAR measurements in eastern Pyrenees, in: Proceedings of the International Snow Science Workshop ISSW 2009 Europe, Davos, Switzerland, 27. September bis 2. Oktober 2009, 202–206, 2009. 3688

Mott, R., Schirmer, M., Bavay, M., Grünewald, T., and Lehning, M.: Understanding snow-transport processes shaping the mountain snow-cover, The Cryosphere, 4, 545–559, doi:10.5194/tc-4-545-2010, 2010. 3668

Mott, R., Scipion, D., Schneebeli, M., Dawes, N., Berne, A., and Lehning, M.: Orographic effects on snow deposition patterns in mountainous terrain, J. Geophys. Res.-Atmos., 119, 1419–1439, doi:10.1002/2013jd019880, 2014. 3666, 3667, 3668, 3669

Peck, E. L. and Brown, M. J.: An approach to the development of isohyetal maps for mountainous areas, J. Geophys. Res., 67, 681–694, doi:10.1029/JZ067i002p00681, 1962. 3667, 3680

Rasmussen, R., Dixon, M., Hage, F., Cole, J., Wade, C., Tuttle, L., McGettigan, S., Carty, T., Stevenson, L., Fellner, W., Knight, S., Karplus, E., and Rehak, N.: Weather support to deicing decision making (WSDDM): a winter weather nowcasting system, B. Am. Meteorol. Soc., 82, 579–595, 2001. 3668

Rasmussen, R. M., Hallett, J., Purcell, R., Landolt, S. D., and Cole, J.: The hotplate precipitation gauge, J. Atmos. Ocean. Tech., 28, 148–164, doi:10.1175/2010jtecha1375.1, 2011. 3668

Robichaud, A. J. and Austin, G. L.: On the modelling of warm orographic rain by the seeder-feeder mechanism, Q. J. Roy. Meteor. Soc., 114, 967–988, doi:10.1002/qj.49711448207, 1988. 3667

TCD
8, 3665–3698, 2014

Rohrer, M., Braun, L., and Lang, H.: Long-term records of snow cover water equivalent in the Swiss Alps 1. Analysis, Nord. Hydrol., 25, 53–64, 1994. 3667, 3680
Sandau, R.: Digital Airborne Camera. Introduction and Technology, Springer, Heidelberg, Germany, 2010. 3671
Schirmer, M., Wirz, V., Clifton, A., and Lehning, M.: Persistence in intra-annual snow depth distribution: 1 Measurements and topographic control, Water Resour. Res., 47, W09516, doi:10.1029/2010wr009426, 2011. 3672, 3682
Scipion, D. E., Mott, R., Lehning, M., Schneebeli, M., and Berne, A.: Seasonal small-scale spatial variability in alpine snowfall and snow accumulation, Water Resour. Res., 49, 1446–1457, doi:10.1002/wrcr.20135, 2013. 3668, 3669
Sevruk, B.: Regional dependency of precipitation-altitude relationship in the Swiss Alps, Climatic Change, 36, 355–369, 1997. 3667, 3668, 3680
Spreen, W.: A determination of the effect of topography upon precipitation, T. Am. Geophys. Un., 28, 285–290, 1947. 3667, 3680
Trujillo, E., Ramirez, J. A., and Elder, K. J.: Topographic, meteorologic, and canopy controls on the scaling characteristics of the spatial distribution of snow depth fields, Water Resour. Res., 43, 1–17, doi:10.1029/2006WR005317, 2007. 3670
Trujillo, E., Ramirez, J. A., and Elder, K. J.: Scaling properties and spatial organization of snow depth fields in sub-alpine forest and alpine tundra, Hydrol. Process., 23, 1575–1590, doi:10.1002/Hyp.7270, 2009. 3670
Wastl, C. and Zängl, G.: Analysis of mountain-valley precipitation differences in the Alps, Meteorol. Z., 17, 311–321, doi:10.1127/0941-2948/2008/0291, 2008. 3667, 3668, 3680
Wehr, A. and Lohr, U.: Airborne laser scanning – an introduction and overview, J. Photogr. Remote Sens., 54, 68–82, 1999. 3670
Yang, D. Q., Goodison, B. E., Metcalfe, J. R., Golubev, V. S., Bates, R., Pangburn, T., and Hanson, C. L.: Accuracy of NWS 8 standard nonrecording precipitation gauge: results and application of WMO intercomparison, J. Atmos. Ocean. Tech., 15, 54–68, 1998. 3668
Zängl, G.: The temperature dependence of small-scale orographic precipitation enhancement, Q. J. Roy. Meteor. Soc., 134, 1167–1181, doi:10.1002/qj.267, 2008a. 3667
Zängl, G., Aulehner, D., Wastl, C., and Pfeiffer, A.: Small-scale precipitation variability in the Alps: Climatology in comparison with semi-idealized numerical simulations, Q. J. Roy. Meteor. Soc., 134, 1865–1880, doi:10.1002/qj.311, 2008b. 3667

TCD
8, 3665–3698, 2014

Table 1. Data sets analysed in the study where “Date" refers to the date of the winter survey, “Mean acc." to the mean accuracy in vertical direction as denoted in the reference column and “Platform" to the measurement platform.

Name	Date	Mean acc. [m]	Platform	Reference
Dischma valley (DIS) Strela (STRE)	20 Mar 2012	0.3–0.5	Leica ADS80	Bühler et al. (2009, 2014)
Val de Núria (NUR)	9 Mar 2009	0.3	Optech ALTM3025	Moreno Baños et al. (2009)
Hintereisferner (HEF)	7 May 2002	0.3	Optech ALTM1225	Geist and Stötter (2008); Bollmann et al. (2011)
Haut Glacier d'Arolla (ARO)	1 May 2007	0.1	Riegl LMS Q240i-60	Dadic et al. (2010a, b)
Wannengrat (WAN)	26 Apr 2008	0.1	Riegl LMS Q240i-60	Grünewald and Lehning (2011); Lehning et al. (2011)

TCD
8, 3665–3698, 2014

Table 2. Summary statistics and main characteristics of the investigation areas: “Area" is given in km^2, elevation range (EL) in m a.s.l., mean slope (SL) in °, mean and standard deviation (std) of snow depth (HS) in m. Areas with trees and larger vegetation were masked from the data sets.

Name	Location	Area	Elev	SL	Asp	mean HS	std HS	Description
DIS	Davos, Eastern Swiss Alps	78	1760–3146	29	All	1.37	0.95	Mixture of steep and gentle slopes, some rock faces
STRE	Davos, Eastern Swiss Alps	26	1850–2781	29	All	1.77	1.46	Mixture of steep and gentle slopes, some rock faces
NUR	Southeastern Spanish Pyrenees	28	2000–2900	28	All	1.05	1.06	Mixture of gentle slopes and some rock outcrops
HEF	Rofen valley, South-western Austrian Alps	25	2300–3740	24	All	2.09	1.2	50 % glaciers, steep talus and rock-faces
ARO	Valais, Southwestern Swiss Alps	10	2400–3500	28	SW to SE	1.14	0.9	50 % glaciers, steep talus and rock-faces
WAN	Davos, Eastern Swiss Alps	4	1940–2650	27	All	1.48	1.07	Mainly talus slopes, some rocky outcrops and rock-faces in summit region
LAG	Davos, Southeastern Swiss Alps	3	1800–3080	40	SE to SW	1.56	1.41	Steep talus slopes surrounded by rock-faces

TCD
8, 3665–3698, 2014

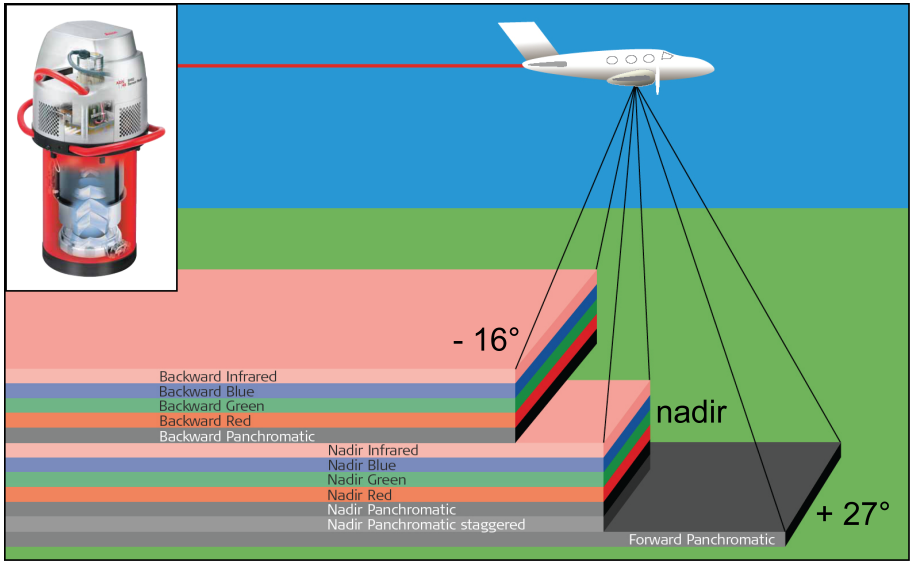

Figure 1. ADS80 sensor (top left) and data acquisition scheme with spectral bands and viewing angles (Source: Bühler et al., 2009).

TCD
8, 3665–3698, 2014

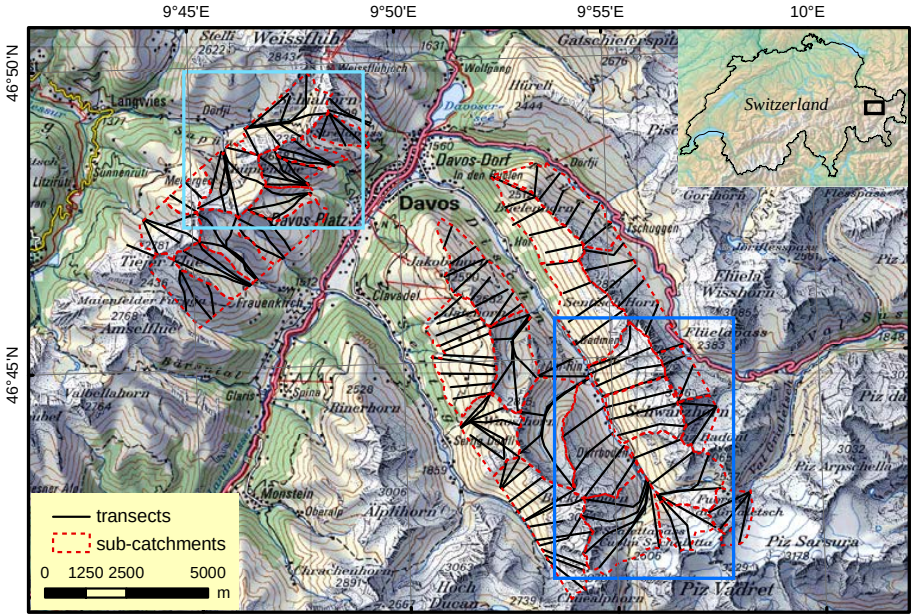

Figure 2. Overview map on the study region DIS and STRE. The upper left panel indicates the position in the East of Switzerland. Detailed views for parts of the domains are shown in Fig. 3. Maps reproduced with permission (Swisstopo, JA100118).

TCD
8, 3665–3698, 2014

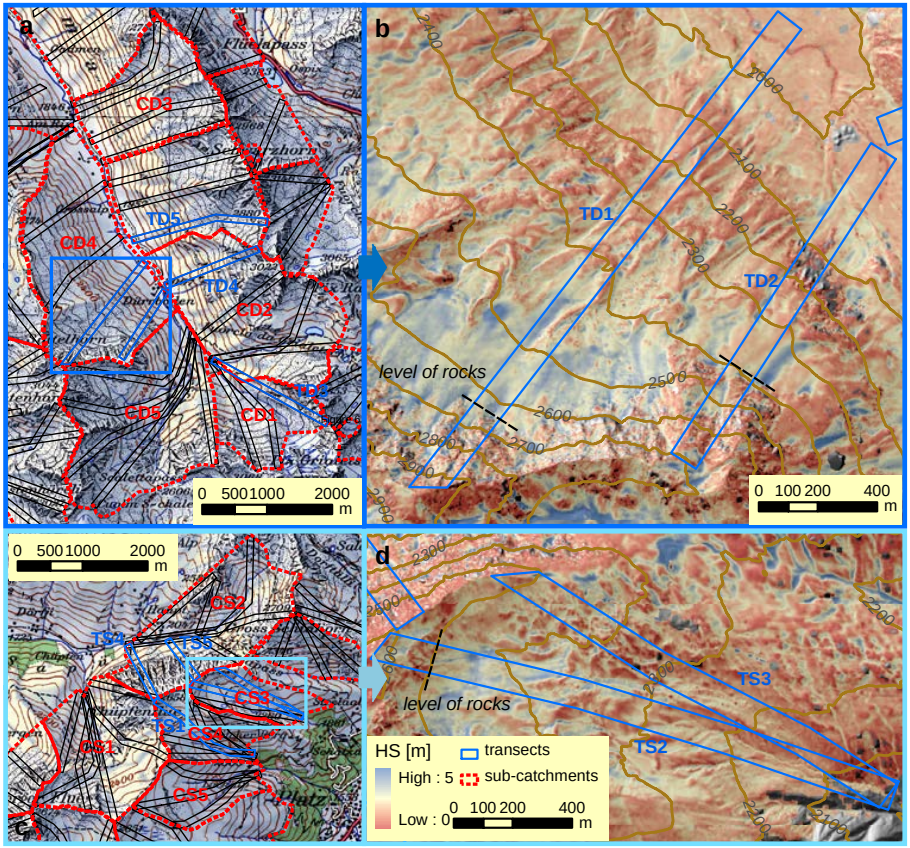

Figure 3. Detailed maps of catchment (CD1–5 and CS1–5 see Fig. 6), and transects (CT1–5 and CS 1–5 see Fig. 7) and discussed in the text. Maps reproduced with permission (Swisstopo, JA100118).

TCD
8, 3665–3698, 2014

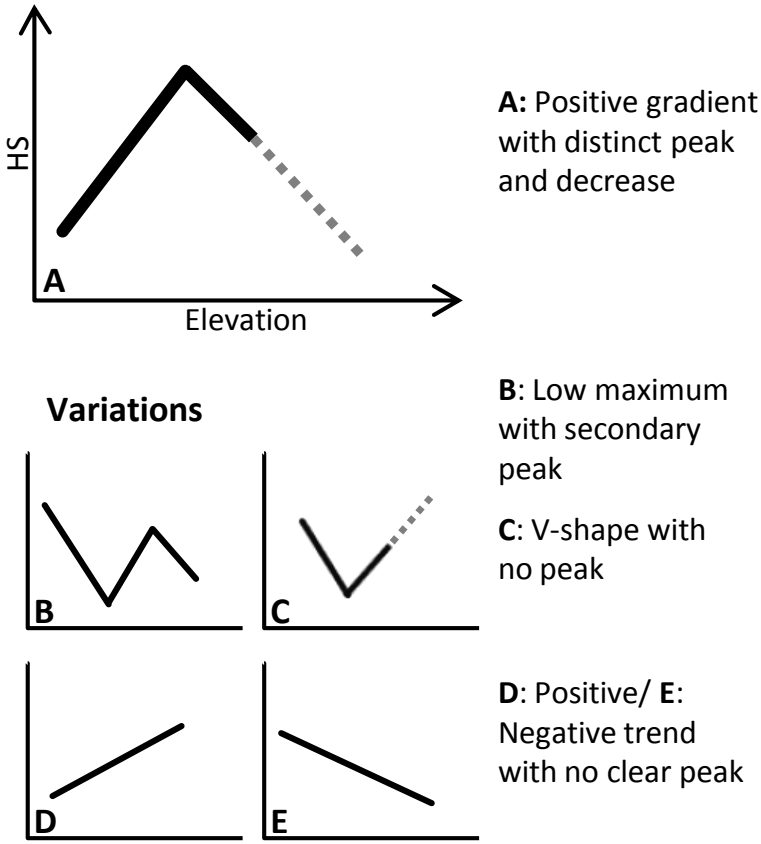

Figure 4. Idealised shape of elevation gradients and variations as identified from the data sets.

TCD
8, 3665–3698, 2014

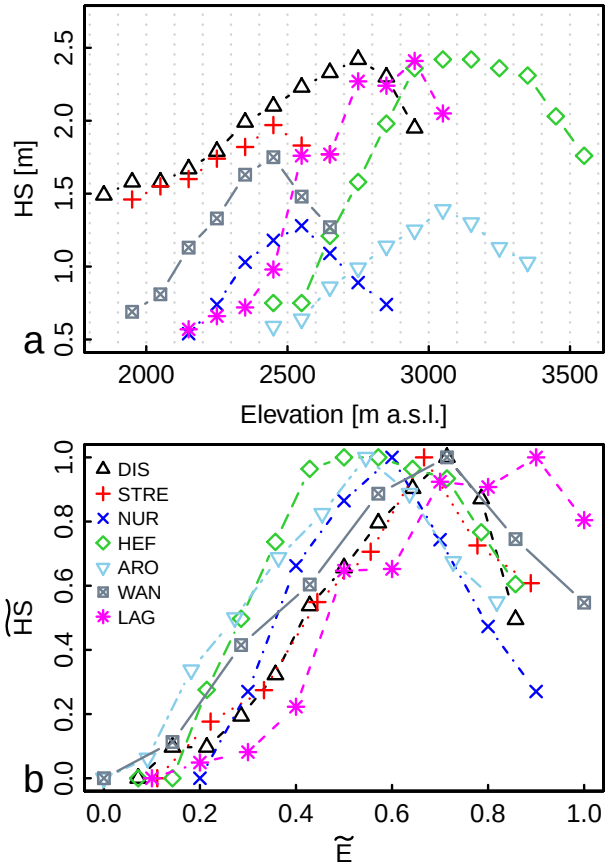

Figure 5. Elevation gradients on the scale of the complete data sets. In **(a)** snow depths are plotted against Elevation as raw values **(b)** and rescaled by applying Eq. (1) to snow depth and elevation.

TCD
8, 3665–3698, 2014

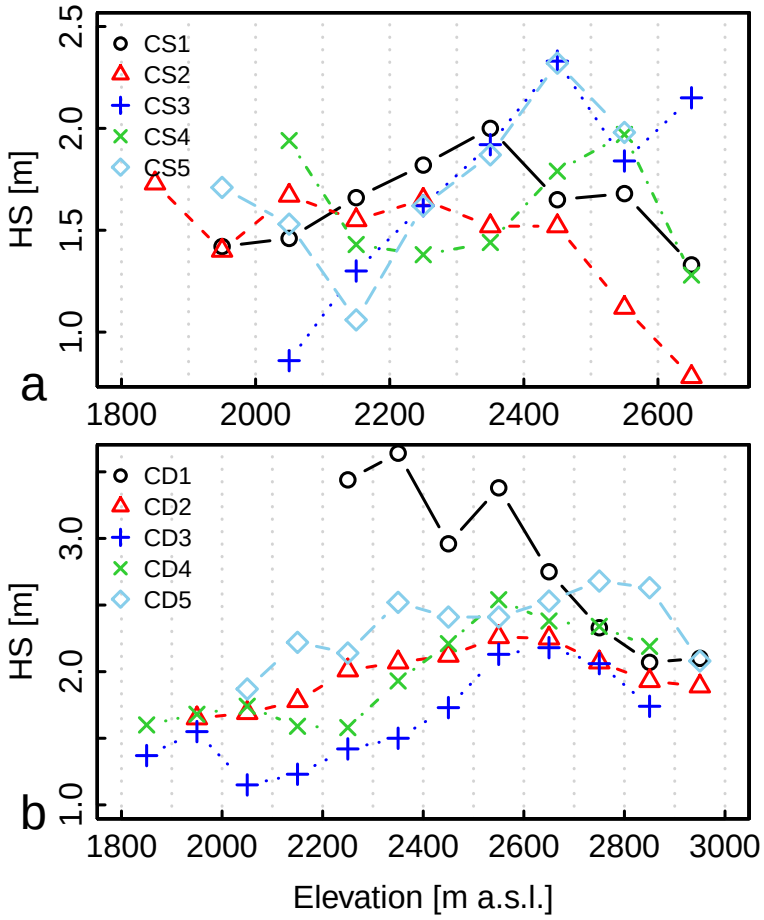

Figure 6. Elevation gradients of selected sub-catchments from the Strela mountain range **(a)** and the Dischma valley **(b)**.

TCD
8, 3665–3698, 2014

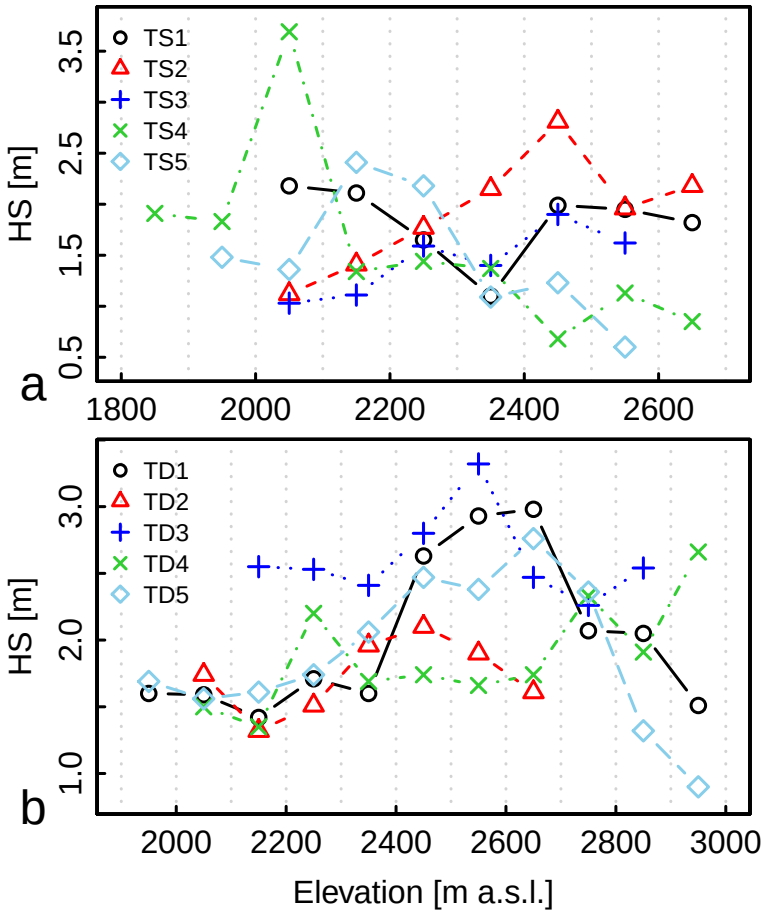

Figure 7. Elevation gradients of selected transects from the Strela mountain range **(a)** and the Dischma valley **(b)**.

TCD
8, 3665–3698, 2014

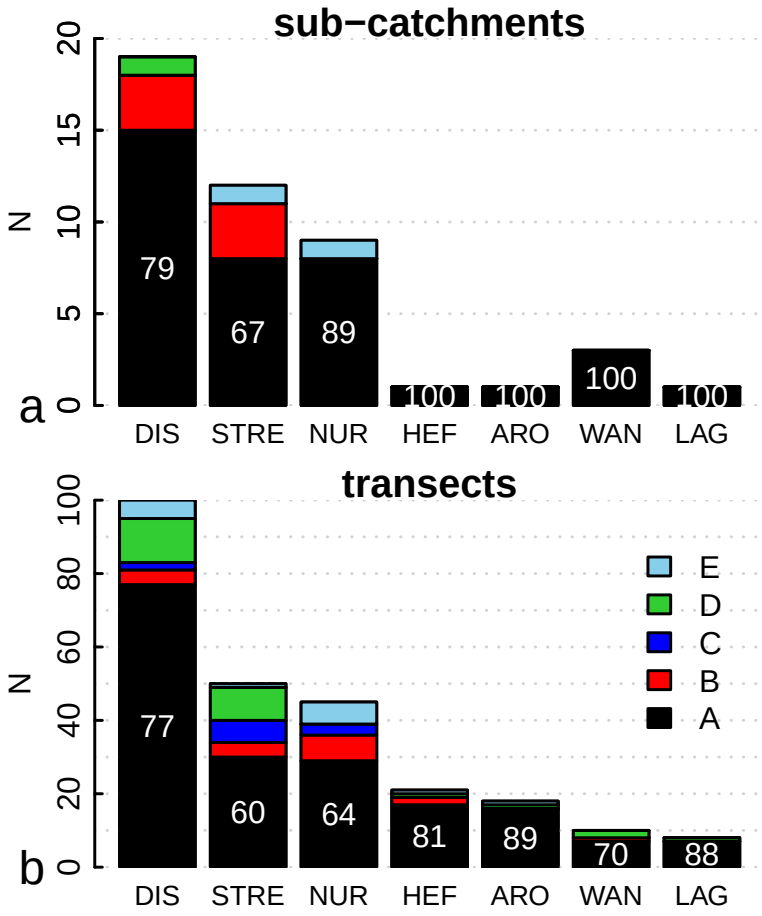

Figure 8. Frequency distribution of the types of gradients (A–B as shown in Fig. 4) for sub-catchments **(a)** and transects **(b)** of each data set. White numbers indicate the percentage of subareas classified as type A.

TCD
8, 3665–3698, 2014

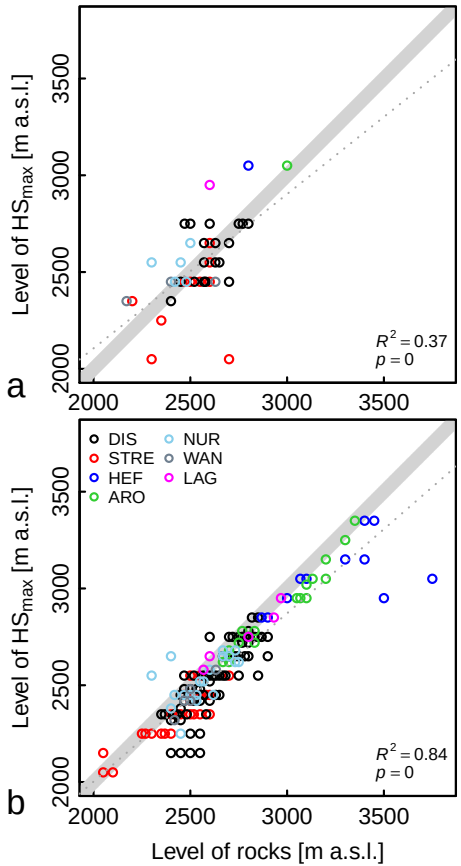

Figure 9. Level of rocks versus level of the maximum of the elevation – snow depth relationship for the transects **(a)** and the sub-catchments **(b)**. The grey shaded area illustrates the 1-1 line (±50 m) and the dashed line the linear fit of the merged data.

TCD
8, 3665–3698, 2014